Žganjar *et al.*
Biotechnology for Biofuels and Bioproducts (2025) 18:112
https://doi.org/10.1186/s13068-025-02713-7

Biotechnology for Biofuels and Bioproducts

RESEARCH

Open Access

Transcriptomics-based analysis of acetate and propionate transport and metabolism in *Yarrowia lipolytica*

Mia Žganjar[1,2], David Sanz-Mata[3], Urška Hancman[4], Neža Čadež[2], Cene Gostinčar[4], Cristina González-Fernández[3,5], Elia Tomás-Pejó[3] and Uroš Petrovič[1,4*]

Abstract

Background *Yarrowia lipolytica* is a promising host for sustainable microbial oil production from waste-derived carboxylic acids such as acetate and propionate. Nonetheless, the molecular mechanisms underlying the metabolism and assimilation of these substrates, particularly under nitrogen limitation, are still not fully understood.

Results We conducted a multi-condition transcriptomic analysis of *Y. lipolytica* strain EXF-17398 under nitrogen-limiting conditions to investigate its transcriptional adaptation to acetate and propionate utilisation. Our results revealed distinct transcriptional responses associated with metabolic adaptation, including the coordinated regulation of Jen and Gpr carboxylate transporter families, suggesting a dual system for carboxylate uptake. *JEN5* and *GPR1* appear central to propionate and acetate utilisation, respectively. Our data suggest that propionate toxicity is mitigated through its conversion via the methylcitrate cycle and potentially the malonate semialdehyde pathway, preventing accumulation of cytotoxic propionyl-CoA in the cytosol. The upregulation of carnitine acyltransferases suggests active mitochondrial transport of acyl-CoAs, linking detoxification with energy metabolism. Under tested conditions, the de novo lipid synthesis was consistent with carbon overflow from acetyl-CoA and propionyl-CoA, supported by intracellular nitrogen recycling and redox balancing, independent of classical nitrogen regulatory pathways.

Conclusions These findings illustrate the capacity of *Y. lipolytica* to coordinate carbon and nitrogen metabolism during carboxylate utilisation, such as acetate and propionate, offering insights to guide the optimisation of microbial oil production from renewable feedstocks.

Keywords *Yarrowia lipolytica*, Acetate, Propionate, Carboxylate transport, RNA-Seq, Lipid accumulation, Nitrogen limitation

*Correspondence:
Uroš Petrovič
uros.petrovic@bf.uni-lj.si
Full list of author information is available at the end of the article

Background

Yarrowia lipolytica is a versatile oleaginous non-conventional yeast capable of utilising various carbon sources and accumulating neutral lipids up to 40–50% (w/w) under nitrogen limitation, with engineered strains in optimised conditions reaching up to 80% (w/w) [1]. In recent years, carboxylic acids have attracted increased attention as sustainable substrates for various microbial fermentation processes [2]. These substrates are readily available from waste-derived feedstocks, presenting an opportunity to valorise organic wastes into valuable microbial oils [3–5]. Converting organic waste into microbial oils via the carboxylate platform thus holds promise for sustainable production of both even- and odd-chain fatty acids (ECFAs and OCFAs), the latter representing high-value compounds used in pharmaceuticals, agrochemicals, flavours, coatings and more [6–8].

The use of alternative carbon sources, such as carboxylic acids, is challenging. Weak carboxylic acids, such as acetate and propionate, can on one side serve as carbon and energy sources but may also impose metabolic stress [9–12]. At low pH, weak acids are in their undissociated form, freely diffusing into the cell, where they dissociate. Anions enter metabolic pathways, while excess protons lead to cytosolic acidification and growth inhibition [13–15]. *Y. lipolytica* mitigates this by buffering protons intracellularly, sequestering them in metabolic reactions, and actively exporting excess protons and anions [14, 15]. At higher extracellular pH, acids shift to their deprotonated form, limiting passive diffusion through the membrane. Their uptake is then tightly regulated by secondary active transport [13, 14, 16].

In oleaginous yeasts, there are two strategies of lipid synthesis. The de novo pathway relies on hydrophilic substrates (e.g., sugars, alcohols), which are converted to fatty acid precursors, such as acetyl-CoA and propionyl-CoA for generation of ECFAs and OCFAs. These precursors are carboxylated by the fatty acid synthase complex and esterified via the Kennedy pathway into triacylglycerols (TAGs). In contrast, the *ex novo* pathway hydrolyses exogenous hydrophobic substrates (e.g., free fatty acids, waste vegetable oils, TAGs) into fatty acids, which are then activated to acyl-CoAs and directly incorporated into TAGs without de novo chain elongation. And while *Y. lipolytica* represents a robust system for microbial oil production with extensive research on its lipid accumulation, the interplay between de novo and *ex novo* routes, coupled with pH-dependent carboxylic acid uptake and their metabolism, remains largely uncharacterised [7, 17–19].

To address this, we selected a strain of *Y. lipolytica*, EXF-17398, as the best performer of a recent large-scale screen of non-conventional yeasts capable of utilising high amounts of carboxylic acids [2]. We performed a transcriptomic analysis of cells cultivated on acetate and propionate as the sole source of carbon and compared them to controls with glucose. All cultures were grown in conditions of nitrogen depletion (C/N ratio of 200:1).

We aimed to identify the propionate and acetate utilisation pathways, determine whether these substrates feed the de novo or the *ex novo* lipid synthesis pathway, and provide insight into how nitrogen limitation modulates carboxylate-driven lipid accumulation. These insights lay the groundwork to enhance the carboxylate-based industrial production of microbial oils in *Y. lipolytica* in the future.

Methods

Strain and culture conditions

Y. lipolytica strain EXF-17398 was obtained from the Culture Collection Ex (part of Infrastructural Centre Mycosmo, MRIC UL, Slovenia) [2] and stored in 30% (v/v) glycerol at − 80 °C until use. Cells were reactivated by cultivation on solid YPD medium (10 g/L yeast extract, 20 g/L peptone, 20 g/L glucose, 20 g/L agar) media at 28 °C.

Shake-flask fermentation

The shake-flask fermentation experiment was performed in 250 mL baffled Erlenmeyer flasks with 100 mL of minimal synthetic medium composed of 17 g/L Yeast Nitrogen Base (YNB) without amino acids with 10 g/L of one of the corresponding carbon sources (glucose, acetic acid, or propionic acid) and under nitrogen-limiting conditions with ammonium sulphate adjusted to a C/N ratio of 200:1. This C/N ratio was selected based on previous studies showing optimal lipid accumulation under nitrogen-limited conditions, typically within the range of 100 to 200 [20]. The initial pH of the medium was adjusted to 6.0 using 3 M NaOH.

Cell growth was followed by a Spectroquant® Pharo 100 spectrophotometer at optical density 600 nm (OD_{600}). The pH was monitored throughout the cultivation period.

Samples for RNA sequencing were collected from 3 biological replicates per cultivation condition and at two time points, resulting in a total of 18 samples. Cells in the exponential growth phase were harvested after 24 h in the case of glucose and acetic acid and after 48 h in the case of propionic acid. The second sampling point was in the stationary growth phase after 144 h for all carbon sources. These time points were selected to capture

both active growth and lipid accumulation phases, as previously described in similar studies [21].

Analytical methods

The substrate consumption profile was analysed by high performance liquid chromatography (HPLC) using the Agilent 1260 HPLC-RID (Agilent, Santa Clara, CA, USA) equipped with a Cation H Refill Cartridge Microguard column (Bio-rad, Hercules, CA, USA) and an Aminex HPX-87H ion exclusion column (300 × 7.8 mm I.D.) (Bio-rad). The mobile phase was 5 mM H_2SO_4, and elution was performed in isocratic mode at a flow rate of 0.6 mL/min. The injected sample volume was 20 µL. The oven and detector were set at 44 °C and 35 °C, respectively.

Whole genome sequencing

The whole genome of *Y. lipolytica* EXF-17398 was sequenced using short-read high-throughput sequencing. The biomass was cultivated in liquid yeast nitrogen base (YNB) medium at 24 °C with constant shaking at 180 rpm. The biomass was homogenised in liquid nitrogen with a pestle and mortar and then additionally ground for 1 min in the Retsch Mixer Mill 301 (ThermoFisher Scientific, Waltham, Massachusetts, USA) at 20 Hz. Total genomic DNA was extracted from the biomass using the UltraClean Microbial DNA isolation kit (MO BIO Laboratories, Carlsbad, California, USA). The isolated DNA was analysed to ensure sufficient quantity and quality using agarose electrophoresis and by fluorometry on Qubit 4 (Thermo Fisher Scientific, Waltham, Massachusetts, USA). The DNA has been sent for sequencing at Novogene on the Illumina platform with a targeted 5 Gbp output of paired-end 150 bp reads.

After the sequencing, the raw reads were processed with fastp (v0.23.4) [22]. The reads were trimmed for quality (phred quality score threshold of 20 in a 3-bp window) and for remaining adapter sequences using the default fastp adapter database. Short reads (< 50 bp) were discarded. Deduplication was performed with the accuracy setting of 5. The remaining reads were assembled with the SPAdes genome assembler (v4.0.0) [23] and the option "–isolate" and other parameters left at default values. Scaffolds or contigs shorter than 1000 bp were removed from the assemblies with SeqKit (v2.8.2) [24]. The assembled genome was inspected with QUAST (v5.2.0) [25].

RNA isolation, RNA sequencing (RNA-Seq) and analysis

The total RNA was extracted using the RNeasy Micro Kit (Qiagen), following the instructions provided by the manufacturer, including the removal of DNA using the RNase-Free DNase Set (Qiagen). The RNA concentration and quality were determined by measuring the 260/280 ratios with SPECTROstar Omega (BMGLABTECH).

The sequencing library was prepared by mRNA poly(A) enrichment, performed by the sequencing provider with the Nextflex Rapid Directional RNA-Seq 2.0 kit and Poly(A) Beads 2.0 (PerkinElmer). mRNA sequencing (mRNA-Seq) was performed on the Illumina NovaSeq 600 with 2 × 150 bp long paired-end run with a sequencing throughput of 20 million paired-end (PE) reads per sample and a quality of Q30 ≥ 80%.

The raw sequencing (.fastq) files of separate sequencing lanes were merged. The fastp tool (v.0.20.1) [22] was then used to perform pre-processing steps, including adapter trimming and quality filtering. Read quality was determined with the FastQC tool (v0.11.9) [26], run prior to and after pre-processing. Contamination quality checks were performed with the FastQ Screen (v0.15.3) tool [27]. Trimmed, high-quality reads were quasi-mapped and quantified using the Salmon tool (v1.10.1) [28]. For this, the *Y. lipolytica* reference strain CLIB122 genome and transcriptome files (ENSEMBL genome assembly ASM252v1, GCA_000002525.1) were used. The Samtools (v1.17) [29] tool was used to convert the Salmon output mappings (.SAM files) to.BAM files. Transcript-level expression abundances (counts) were gene-level summarised using the tximport (v1.26.1) [30] tool as described in the corresponding documentation.

Differential expression analysis (DEA) and functional enrichment

Multi-condition differential expression (DEA) analysis was performed using the DESeq2 tool (v. 1.40.2) [31]. The gene-level raw counts were normalised prior to testing, using normalisation size factors as the default process in DESeq2. Genes with zero counts in all samples, as well as genes with extreme count outliers in at least 3 samples per group and genes with low mean normalised counts (< 10), were filtered out. Then, the gene-wise dispersion was estimated and shrunk automatically. Finally, DESeq2 performed hypothesis testing using the Wald test for pairwise comparisons of known sources of variation, combining the *condition* (carbon source), growth *phase* and their interaction term (*condition:phase*). This was provided by the design formula: ~ *Condition* + *Phase* + *Condition:Phase*. In this case, glucose and the exponential growth phase were set as base levels for group comparisons. An additional DEA was performed, comparing the differential gene expression between propionic and acetic acid at two selected growth phases, where acetic acid and the exponential growth phase were selected as the baseline condition. The significance threshold was set to alpha = 0.05, and the p-values were adjusted based on the Benjamini and Hochberg (BH)

algorithm (p_{adj}). Genes with $|\log_2 FC| > 1$ and $p_{adj} \leq 0.05$ were considered to be significantly differentially expressed genes (DEGs). In total, 7 contrasts were specified for sample group inspection: P versus G, A versus G, and P versus A, for comparison of differences between carbon sources (*A*-acetic acid, *P*-propionic acid, and G-glucose). S versus E for inspecting differences between stationary and exponential growth phases (*E*-exponential phase, *S*-stationary phase). The interaction term contrasts AS versus AE, PS versus PE and PS versus PE (a) correspond to differences between carbon sources and growth phases by stabilising the base condition as described above. Obtained expression values are available in Supplementary S2.

The over-representation analysis (ORA) was performed by determining the enriched gene ontology (GO) terms and Kyoto Encyclopaedia of Genes and Genomes (KEGG) pathways for DEGs per contrast. For this, genekitr (v.1.2.5) [32] and clusterProfiler (v.4.8.3) [33] tools were used. The functional enrichment was also performed on the GO Slim yeast (*Saccharomyces cerevisiae*) subset terms. The significance threshold was again set to alpha = 0.05, and the p-values were BH adjusted. Terms with $p_{adj} \leq 0.05$ were considered to be significant. The annotation coverage of GO Slim terms was calculated for each DEA contrast by determining the proportion of DEGs that were mapped to at least one GO Slim term and for the whole set of genes included in the transcriptomic analysis.

Key metabolic pathways were retrieved from the KEGG database and mapped with expression (log2FC) values, categorised into preset intervals. Gene symbols were retrieved from literature and, in some cases, based on *S. cerevisiae* homology.

Computational analysis

The DNA and protein sequences of candidate transporter genes (Supplementary S1 Table S1) of *Y. lipolytica* strain EXF-17398 were extracted from the WGS assembled sequence. Protein sequences were aligned using the MUSCLE algorithm in MEGA (v. 11.0.13) [34] with default parameters to ensure accurate identification of conserved motifs. A phylogenetic tree was constructed using the Maximum Likelihood (ML) method with the Jones-Taylor-Thornton (JTT) model. The reliability of the tree topology was assessed with 1000 bootstrap replicates. The tree was visualised using the ggtree (v. 3.14.0) [35] R package.

The transmembrane domains were predicted using the DeepTMHMM (v. 1.0.32) [36] tool. They were further analysed based on their AlphaFold protein structure and TM topology using the Membranefold tool (v. 0.071) [37], which also predicts the cellular environment for each protein residue. Conserved motifs and the multiple sequence alignment were visualised using the ggmsa (v. 1.12.0) [38] and the ragp (v. 0.3.5.9) [39] R packages. The subcellular location of proteins was checked using the TargetP 2.0 tool (v. 2.0) [40].

Results

RNA sequencing and differential gene expression analysis

A graphical representation of our experimental approach is shown in Fig. 1a. The selected *Y. lipolytica* strain EXF-17398 was cultivated in liquid nitrogen-limiting media with either acetic or propionic acid as the sole source of carbon. A medium with glucose was chosen as a control. Cells were harvested at two time points: in the exponential and in the transition growth phase preceding the stationary phase (hereafter termed the stationary

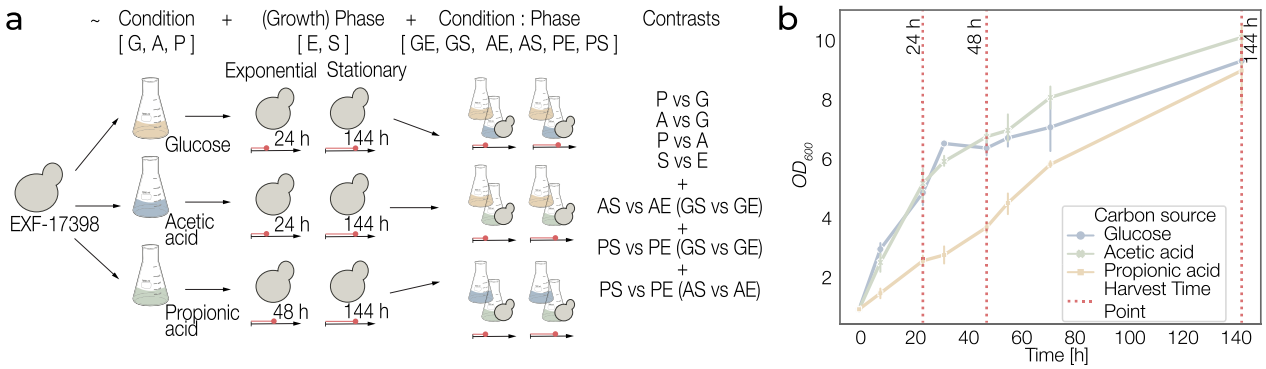

Fig. 1 Experimental design and growth dynamics of the *Yarrowia lipolytica* strain EXF17398. **a** Overview of the experimental design for differential expression analysis (DEA), illustrating the tested carbon source conditions (glucose (G), acetic acid (A), and propionic acid (P)), growth phases (exponential (E) and stationary (S)), and corresponding sampling time points (24 h—acetic acid and glucose, 48 h—for propionic acid, and 144 h—for all conditions; red dashed lines). The design formula for DEA contrasts is shown, highlighting the comparisons between conditions, phases, and their interactions (Condition, Phase, and Condition:Phase terms). b) Growth curves of *Y. lipolytica* strain EXF17398 under tested carbon sources, with specified sampling time points (24, 48, and 144 h, see above)

growth phase, as cell division had largely ceased). During the exponential growth phase, yeast cells displayed rapid growth on acetic acid and glucose, whereas growth on propionic acid was slower. Between the two sampling points, growth on propionic acid accelerated, resulting in a more comparable dynamic across all conditions (Fig. 1b). This growth pattern was reflected in the carbon utilisation profiles, pH dynamics, and final optical densities (OD_{600}) at the sampling time points (Fig. 1b, Table 1 and Additional file 1 Figure S1).

The fastest overall growth was observed by utilising acetic acid, with the highest maximal OD_{600} value of 10.18 ± 0.1 and the carbon consumption level of up to 74% in the stationary phase. Glucose and propionic acid consumptions in the stationary phase were 67% and 62%, respectively, with OD_{600} values up to 9.38 ± 0.52 for glucose and 9.06 ± 1.41 for propionic acid. In the exponential growth phase, carbon source consumption was consistent across all conditions and was around 30%. The pH at harvest varied across conditions, with glucose cultures having the most acidic final pH (4.0), while cultivations on acetic and propionic acid resulted in alkaline pH values (8–10).

To understand how carbon source influences growth and lipid biosynthesis, we examined gene expression profiles to identify condition- and growth phase-dependent effects. Principal component analysis (PCA) revealed clear sample separation driven by growth phase and condition, with biological replicates forming tight groups. Samples primarily clustered by condition along PC1, which explains 77.46% of the total variance and separates glucose from acid-based conditions, while variation related to growth phase is reflected along PC2, accounting for 14.62% of the variance. Notably, samples from the propionic acid exponential phase (PE) separated distinctly from other groups, indicating distinct gene expression patterns (Additional file 1 Figure S2a). Given the condition- and the growth phase-dependent transcriptional differences indicated by the PCA, we performed a multi-condition differential expression analysis (DEA). Specifically, we employed a design formula that included the main effects of carbon source (Condition) and growth phase (Phase), along with their interaction (Condition:Phase) (Fig. 1a). Glucose and the exponential phase were used as the initial baseline, followed by acetic acid and the exponential phase for the second analysis. Seven contrasts were specified, with direct comparisons (P vs. G, A vs. G, P vs. A, S vs. E) and interaction contrasts (AS vs. AE, PS vs. PE, PS vs. PE_a) that adjust for baseline shifts across carbon sources and growth phases. Notably, PS versus PE uses glucose in the exponential phase as the baseline condition, while PS versus PE_a uses acetic acid in the exponential phase as the baseline.

Differences in gene expression

In the DEA, we examined a total of 6041 genes, with direct comparisons of propionic acid to glucose (P vs. G) and to acetic acid (P vs. A) showing the most altered transcriptomic profiles. These contrasts had the highest proportions of differentially expressed genes (DEGs), accounting for 23% (1381 DEGs) and 18% (1081 DEGs) of all analysed genes, respectively. Both contrasts also had the highest proportions of upregulated DEGs, with 13% (796 genes) in P versus G and 13% (757 genes) in P versus A. By comparison, other contrasts, such as A versus G and propionic acid in stationary phase (PS) versus in exponential phase (PE), showed fewer DEGs, accounting for 11% (659 genes) and 14% (832 genes), respectively. The smallest differences were observed in direct comparisons of growth phases in the glucose medium (S vs. E), with only 456 DEGs (8%) identified (Additional file 1 Table S1).

The intersection of DEGs across contrasts shows notable overlaps, mirroring the condition- and phase-dependent clustering observed in the PCA (Additional file 1 Figure S2b). Several large intersection sets involve propionic acid contrasts (P vs. G and P vs. A), indicating a core subset of genes is consistently differentially expressed when yeast is grown on this carbon source.

Table 1 Carbon source consumption, OD_{600}, and pH dynamics during growth of Yarrowia lipolytica strain EXF-17398

Carbon source	Growth phase	pH at start	pH at sampling point	Carbon source (g/L) at start	Carbon source (g/L) at sampling point	Consumption (g/L)	Consumption (%)	OD_{600} at sampling point
Glucose	Exponential	6	4	11.42	7.99 ± 0.03	3.43 ± 0.03	30.0	4.93 ± 0.1
	Stationary		4		3.72 ± 0.2	7.7 ± 0.2	67.4	9.38 ± 0.52
Acetic acid	Exponential	6	8	9.84	6.88 ± 0.04	2.96 ± 0.04	30.1	4.84 ± 1.02
	Stationary		10		2.55 ± 0.02	7.29 ± 0.02	74.1	10.18 ± 0.1
Propionic acid	Exponential	6	7	9.42	6.45 ± 0.11	2.96 ± 0.11	31.4	3.67 ± 0.31
	Stationary		10		3.56 ± 0.09	5.86 ± 0.09	62.2	9.06 ± 1.41

The overlap between P versus G and A versus G is also pronounced, suggesting both acids induce some shared transcriptional response distinct from glucose-dependent growth, underscoring the stronger influence of carbon source over the growth phase.

Gene ontology (GO) and GO-Slim functional enrichment

To explore the functional roles of detected DEGs in *Y. lipolytica*, we performed gene ontology (GO)-Slim term over-representation analysis (ORA) for molecular function (MF) (Fig. 2) and biological process (BP) ontologies, using the Yeast GO-Slim subset (Additional file 1 Figure S3). The GO-Slim annotation coverage for the background set of 6041 genes used in the DEA was 81.4%, indicating that most genes are annotated with at least one GO-Slim term. For DEGs, coverage was slightly lower (68–76% across contrasts), consistent with the expectation that not all DEGs are well-annotated.

In the MF ontology, *transmembrane transporter activity* was consistently upregulated in comparisons involving propionic acid (P vs. G and P vs. A), suggesting enhanced transporter activity during growth on propionic acid. Similarly, *oxidoreductase activity* and *hydrolase activity* were enriched (Fig. 2). The BP ontology terms further emphasised condition-specific metabolic changes, with upregulated processes including *transmembrane transport* and *lipid metabolic processes* during growth on propionic or acetic acid. In contrast, terms associated with ribosome biogenesis, such as *rRNA processing*, *ribosomal subunit assembly*, and *RNA modification*, were downregulated across multiple contrasts, indicating reduced translational activity. Processes like *monocarboxylic acid metabolism* and *amino acid transport/metabolism* were also enriched. Growth phase comparisons (S vs. E) of glucose medium showed minimal enrichment of transport-related terms, consistent with smaller transcriptomic differences between phases (Additional file 1 Figure S3). These GO-Slim results provide insight into the broad functional roles of DEGs, highlighting

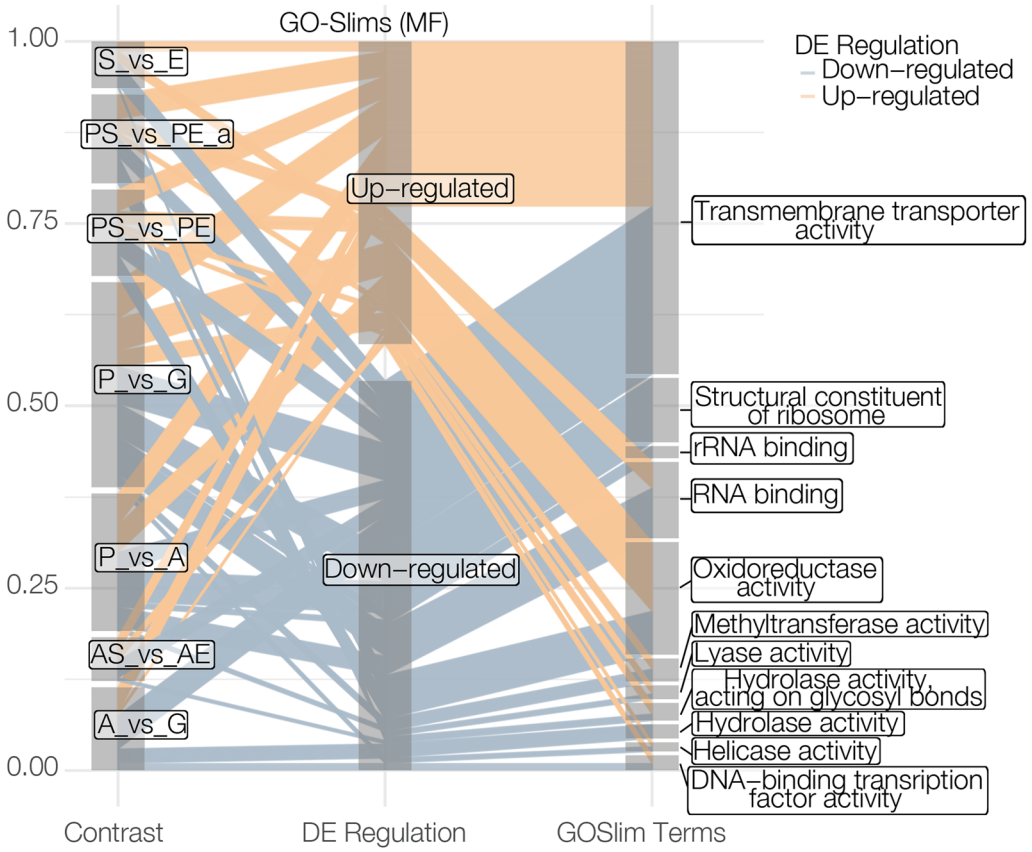

Fig. 2 Overview of gene expression patterns and enriched yeast GO Slim molecular function (MF) terms. A parallel coordinate plot illustrating the functional enrichment of differentially expressed (DE) genes based on the *Saccharomyces cerevisiae* Yeast Gene Ontology (GO) Slim subset of terms for Molecular Function (MF). Over-representation analysis (ORA) was conducted with a significance threshold of adjusted $p < 0.05$. The plot connects proportions of DE genes (left axis) across contrasts (*A*-acetate, *P*-propionate, *G*-glucose, *S*-stationary growth phase, *E*-exponential growth phase) to their regulatory patterns (middle axis, up-regulated or down-regulated genes) and significantly enriched GO Slim MF terms (right axis)

gene regulation patterns and linking them to metabolic adaptation strategies.

To explore the functional space of DEGs in more detail, we also performed ORA of GO terms specific to *Y. lipolytica* (Additional file 1 Figure S4). Consistent with findings from the GO-Slim analysis, transport-related terms were significantly enriched across multiple contrasts. Terms such as *transporter activity*, *transmembrane transporter activity*, *organic acid transmembrane transporter activity*, and *carboxylic acid transmembrane transporter activity* were particularly enriched in propionic acid-based comparisons (P vs. G, P vs. A, PS vs. PE, and PS vs. PE_a). Additional enriched terms, including *symporter activity, solute:proton symporter activity*, and *solute:monoatomic cation symporter activity,* point to mechanisms facilitating ion exchange and metabolite uptake. In growth phase-specific contrasts (S vs. E), transport-related enrichment was less pronounced, but terms such as *metal ion transmembrane transport* and *proton symport activity* suggest regulatory adjustments of ion exchange and pH homeostasis.

Expression patterns of candidate transporters

Since transport-related terms were enriched and the mechanisms of propionate and acetate uptake are not fully understood, we refined our search to identify potential transporter genes. To achieve this, we filtered DEGs annotated with the GO-Slim MF term *transmembrane transporter activity* and further narrowed the selection to DEGs directly or indirectly associated with fatty acid or carboxylate transport, using *Y. lipolytica*-specific GO MF terms (Fig. 3).

Among the identified DEGs, 6 paralogous genes from the Jen gene family of mono-/dicarboxylate transporter were detected, namely *JEN1* (*YALI0C15488g*), *JEN2* (*YALI0C21406g*), *JEN3* (*YALI0D20108g*), *JEN4* (*YALI0D24607g*), *JEN5* (*YALI0B19470g*), and *JEN6* (*YALI0E32901g*) [16, 41]. All these 6 genes were differentially expressed in the P versus G contrast, while 4 of them (*JEN5*, *JEN2*, *JEN1*, and *JEN6*) were also differentially expressed in A versus G, showing a consistent pattern between the acetic and propionic acid conditions. Among them, *JEN5* was one of the most highly upregulated genes, showing strong induction in P versus G ($\log_2$FC = 10.7) and moderate upregulation in A versus G ($\log_2$FC = 7.0) and P versus A ($\log_2$FC = 3.8). Additionally, two other paralogs (*JEN4* and *JEN3*) were slightly to moderately upregulated in the P versus G contrast ($\log_2$FC = 1.4 and 4.3, respectively). In contrast, *JEN6* and *JEN1* were downregulated in both acetic and propionic acid conditions compared to glucose. Gene *JEN6* showed $\log_2$FC values of − 13.9 (A vs. G) and − 10.0

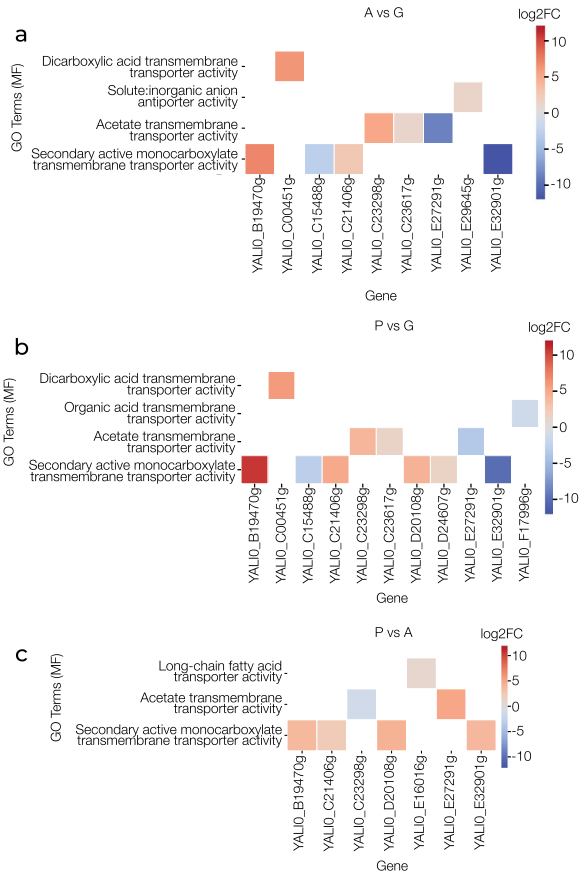

Fig. 3 Condition-based comparisons of differentially expressed genes linked to carboxylic and fatty acid transmembrane transporter activity. Log2 fold change (log2FC) values for gene expression are mapped to enriched Gene Ontology (GO) molecular function (MF) terms of *Yarrowia lipolytica*, specifically related to GO terms of carboxylic and fatty acid transmembrane transporter activity. Genes shown were specifically selected based on GO annotations associated with carboxylate and fatty acid transport. Over-representation analysis (ORA) was performed with a significance threshold of adjusted $p < 0.05$. Panels **a, b,** and **c** illustrate the differential expression analysis (DEA) comparisons of A versus G, P versus G, and P versus A, respectively (*A*-acetate, *P*-propionate, *G*-glucose)

(P vs. G), while *JEN1* had the $\log_2$FC value of − 2.9 in both A versus G and P versus G contrasts.

Beyond the Jen gene family, other transport-related genes were differentially expressed in response to acetic and propionic acid. These were the glyoxylate pathway regulator gene *GPR1* (*YALI0C23617g*) and two of its paralogs, *GPR2* (*YALI0E27291g*) and *GPR6* (*YALI0C23298g*) (Fig. 3), which are linked to acetic acid transport and adaptation [42–46]. Their expression profiles were consistent between the A versus G and P versus G contrasts. *GPR1* and *GPR6* were upregulated, with $\log_2$FC values of 1.2 (A vs. G) and 1.3 (P vs. G) for

GPR1 and $\log_2$FC values of 5.1 (A vs. G) and 4.0 (P vs. G) for *GPR6*. In contrast, *GPR2* showed moderate to strong downregulation with $\log_2$ FC = −3.5 (P vs. G) and $\log_2$ FC = −8.7 (A vs. G). Additionally, gene *YALI0C00451g*, ortholog of *S. cerevisiae DIP5*, a dicarboxylic amino acid permease involved in *L*-glutamate and *L*-aspartate transport, was notably induced with $\log_2$FC values of 5.9 in P versus G and 6.1 in A versus G.

Structural analysis of Jen transporters in *Y. lipolytica* strain EXF-17398

Given the differential expression patterns of the Jen gene family, we further investigated their protein structural properties through protein sequence analysis (Fig. 4, Additional file 1 Figures S5 and S6). Multiple sequence alignment and transmembrane topology predictions of Jen proteins confirmed that all 6 transporters possess 12 transmembrane (TM) α-helices arranged in a twofold semi-symmetrical barrel structure, alternating between intracellular and extracellular regions (Fig. 4, Additional file 1 Figures S5 and S6). The pseudosymmetrical structure is made up of two domains, each with two inverted repeats of 3 α-helices. The N-terminal domain consists of TMs 1–6, while the *C*-terminal domain consists of TMs 7–12. These features are characteristic of transporters in the Sialate:H^+ Symporter (SHS) protein family (TCDB 2.A.1.12) within the Major Facilitator Superfamily (MFS), a diverse group of secondary carriers, among other, known for their role in mono- and dicarboxylate transport [16, 41, 47–49]. Previous work on *Y. lipolytica* Jen transporters reported only 10 TM domains [16, 41, 49], whereas our analysis identified 12 of them. This revised topology aligns with the structural characteristics of other fungal Jen homologs and supports a more conserved architecture within the MFS transporters [47, 50–53]. The conserved sequence motif NXX(S/T)HX(S/T)QDXXXT within TM7 has been previously identified in several fungal Jen transporters and was linked to substrate binding and the proton-coupled symport [54, 55]. This motif is present in all 6 paralogs except for Jen5, where the first S/T residue is substituted by alanine (Fig. 4a). Additionally, the highly conserved residue Q498 in TM11, implicated in monocarboxylate and dicarboxylate discrimination and substrate specificity [51], was also retained across all *Y. lipolytica* paralogs. Notably, Jen5 exhibited another unique structural feature—an extended intracellular loop between TM6 and TM7 [41], potentially influencing its transport function, substrate specificity, and/or regulatory mechanisms (Fig. 4a).

The phylogenetic analysis of *Y. lipolytica* strain EXF-17398 Jen transporters support previously described clustering patterns [16, 41, 50, 53, 54], with Jen5 (YALI0B19470p) forming the most divergent branch (Fig. 4a). The remaining transporters form two distinct subgroups: Jen4 (YALI0D24607p) and Jen3 (YALI0D20108p) cluster together, while Jen2 (YALI0C21406p) and Jen1 (YALI0C15488p) form a separate subgroup. Jen6 (YALI0E32901p) clusters separately from both subgroups, indicating a greater degree of sequence divergence. Additionally, *Y. lipolytica* Jen transporters show higher similarity to each other than to homologs from other yeasts [41, 50]. Whole-genome duplication (WGD) significantly influenced the Jen transporter evolution in yeasts, leading to the loss of Jen2 in WGD yeast species, such as *S. cerevisiae*. In contrast, some non-WGD yeasts, like *Kluyveromyces lactis* and *Candida albicans* [16, 41], retained both Jen1 and Jen2, enabling them to transport both monocarboxylates (Jen1) and dicarboxylates (Jen2). *Pichia kudriavzevii*, on the other hand, has two Jen2 transporters (*PkJen2-1* and *PkJen2-2*) and thus lost Jen1 [50]. However, phylogenomic analyses established that all *Y. lipolytica* Jen transporters form a distinct monophyletic clade (Jen3), separate from the Jen1 and Jen2 clades. These Jen3 transporters likely arose from a common ancestor shared by Jen1 and Jen2, but Jen3 diverged through *Yarrowia* clade-specific expansion events [41, 50, 53]. Their distinct evolutionary adaptation was linked to their broader substrate specificity [41].

Functional enrichment of Kyoto encyclopaedia of genes and genomes (KEGG) pathways

To gain a broader understanding of the metabolic mechanisms underlying acetate and propionate metabolism, we performed an ORA based on Kyoto Encyclopaedia of Genes and Genomes (KEGG) pathways (Additional file 1 Figure S7). In the A versus G comparison, upregulated genes were predominantly linked to *pyruvate metabolism* (8 of 47 genes in the pathway), *glyoxylate/dicarboxylate metabolism* (8 of 36 genes in the pathway), and *fatty acid degradation* (8 of 47 genes in the pathway), suggesting increased oxidative and anaplerotic fluxes in acetate-grown cells. These findings, together with enrichment in *glycolysis/gluconeogenesis* (8 of 37 genes in the pathway), highlight a shift in central carbon metabolism. By contrast, the P versus G condition showed significant enrichment in *propanoate metabolism* (15 of 30 genes in the pathway), *fatty acid metabolism* (11 of 26 genes in the pathway), and *branched-chain amino acid (BCAA) catabolism* (20 of 26 genes in the pathway). Finally, the P versus A comparison revealed enrichment in *DNA replication* (16 of 42 genes in the pathway), BCAA degradation (18 of 26

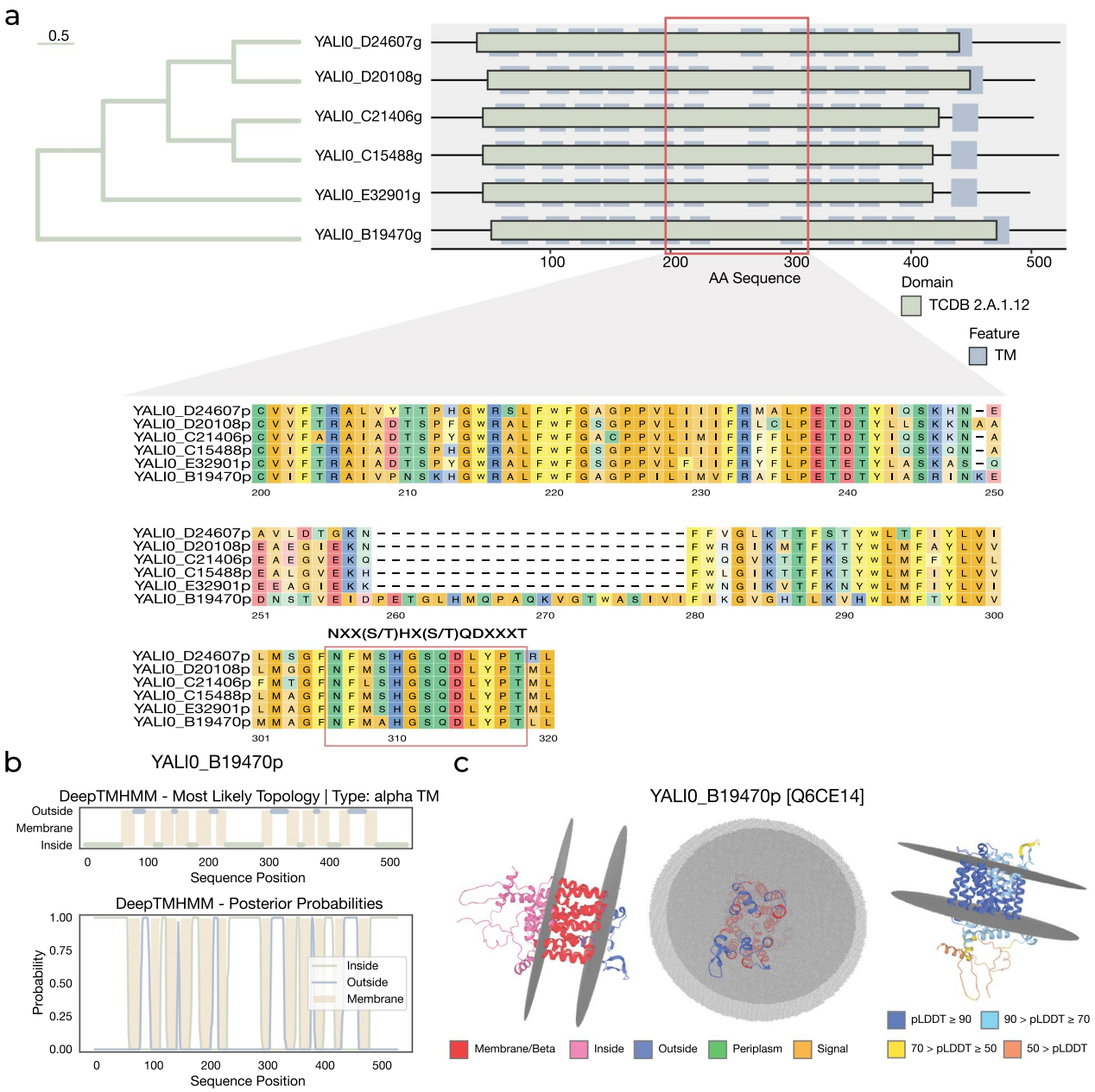

Fig. 4 Phylogenetic, structural, and topological analysis of candidate carboxylate transporters. **a** Phylogenetic tree and sequence alignment of candidate carboxylate transporters, showing the domain architecture and transmembrane (TM) regions. The TCDB 2.A.1.12 protein family domain corresponds to the sialate:H^+ symporter family of major facilitator superfamily (MFS) transporters. TM regions are highlighted, and a detailed alignment of residues 200–320 reveals the key conserved sequence motif NXX(S/T)HX(S/T)QDXXXT within TM7 across the proteins. **b** Predicted transmembrane topology (DeepTMHMM) of YALI0_B19470p, showing the most likely topology and posterior probabilities for sequence positions. The TM regions and their orientations (inside, outside, membrane) are indicated. **c** MembraneFold-predicted structure of YALI0_B19470p, showing the membrane-spanning regions (left, red) and periplasmic/extracellular domains, with pLDDT confidence scores annotated to the AlphaFold predicted structure (right). A cross-sectional view of the predicted membrane embedding is also presented (middle)

genes in the pathway), *propanoate metabolism* (13 of 30 genes), and *glyoxylate/dicarboxylate metabolism* (15 of 36 genes in the pathway).

Inspection of key metabolic pathways

To contextualise enriched KEGG pathways, we integrated key metabolic pathways with associated enzymes and mapped them with expression change values (log2FC) (Fig. 5, Additional file 1 Figure S8, Additional file 2). In this chapter, gene expression changes are presented in terms of relevant DEA contrasts: the propionate condition corresponds to P versus G, the acetate condition to A versus G, and any comparisons between these two correspond to the P versus A contrast.

While our results indicate that propionate and acetate may be transported by Jen and/or Gpr transport systems, their activation to propionyl-CoA and acetyl-CoA is most likely mediated by the sole cytosolic acetyl-CoA synthetase encoded by *ACS1* (*YALI0F05962g*). Its upregulation during growth on propionic or acetic acid, relative to glucose, highlights its dual role in activating both, which was already established for *ScACS1* in *S. cerevisiae* [9, 56, 57]. The transport of CoA derivatives then relies on the mitochondrial carriers, such as carnitine/acetyl-carnitine transporters of the carnitine shuttle, transporting acyl-CoAs, particularly from peroxisomes to mitochondria [11, 58, 59]. Mitochondrial and peroxisomal carnitine acyltransferase encoded by *CAT2* (*YALI0B10340g*) and the cytosolic carnitine acyltransferase encoded by *YAT2* (*YALI0F21197g*) were upregulated in the propionate condition, while *CRC1* (*YALI0C02431g*) and its ortholog *YALI0A20988g* showed no differential expression (Fig. 5).

Our data suggest propionyl-CoA is transported to mitochondria, where it then enters the methylcitrate cycle (MCC). Key MCC enzymes encoded by *CIT1* (*YALI0E00638g*), *PDH1* (*YALI0F02497g*), *ACO1* (*YALI0D09361g*), and *ICL2* (*YALI0F31999g*) were induced in both acetate and propionate conditions (Fig. 5). However, propionate-grown cells showed a more pronounced induction of these enzymes compared to acetate and glucose. Meanwhile, the expression of most tricarboxylic acid cycle (TCA) genes remained unchanged, except for *ACO1* (*YALI0D09361g*) and *IDP1* (*YALI0F04095g*), which were upregulated in both acid conditions. Similar upregulation was observed for most genes of the glyoxylate cycle, with a particularly high upregulation of the malate synthase gene *MLS1* (*YALI0D19140g*). On the other hand, genes encoding key enzymes of the malate-citrate cycle, like *MDH2* (*YALI0E14190g*) and *PYC1* (*YALI0C24101g*), were upregulated only in the propionate condition (Fig. 5).

Interestingly, two genes encoding key enzymes of the the malonate semialdehyde pathway–the 3-hydroxypropionate dehydrogenase gene *HPDH* (*YALI0F02607g*) and the methyl-malonate semialdehyde dehydrogenase gene *MMSDH* (*YALI0C01859g*)–were exclusively upregulated under the propionate condition (Fig. 5, Additional file 1 Figure S8a). For both enzymes a mitochondrial targeting peptide was determined (likelihood of 0.98 and 0.9995, respectively), pointing to a possible propionate detoxification strategy in the mitochondrion. What is more, propionyl-CoA can also arise from the degradation of branched-chain amino acids (BCAAs) [11, 60, 61]. Most genes of the valine, leucine, and isoleucine degradation pathways, including *HPDH* and *MMSDH*, were also exclusively induced under the propionate condition (Additional file 1 Figure S8a). This was also observed for the β-oxidation multifunction enzyme gene *MFE2* (*YALI0B10406g*), whereas *POX2* (*YALI0C23859g*) increased in both conditions (Fig. 5). Activity of β-oxidation is further evident from the upregulation of some acyl/aryl-CoA ligases and canonical acyl-CoA synthetases (ACSs), necessary for fatty acid activation prior to fatty acid oxidation [62]. Again, an exclusive upregulation during growth on propionate was observed for *AAL2* (*YALI0A14234g*), *AAL9* (*YALI0A15103g*) and *FAT3-4* (*YALI0B05456g* and *YALI0C09284g*), as well as for the gene encoding the ATP transporter feeding the AALs, the *ANT1* (*YALI0E03058g*). The acyl/aryl-CoA ligase gene *AAL10* (*YALI0D17314g*) was upregulated in acetate, while the upregulation of *AAL3* (*YALI0E05951g*) was observed in both acid conditions (Fig. 5).

Despite elevated expression of the core fatty acid synthesis genes *FAS1* (*YALI0B15059g*), *FAS2* (*YALI0B19382g*), and *ACC1* (*YALI0C11407g*), most lipid elongation and storage genes remained constantly transcribed (Fig. 5). An exception was *FAD2* (*YALI0B10153g*), which was induced in both acid-based

(See figure on next page.)

Fig. 5 Schematic overview of gene expression changes across metabolic pathways. Metabolic map of *Yarrowia lipolytica* illustrating central carbon metabolism (e.g., tricarboxylic acid cycle (TCA), pyruvate bypass and glyoxylate cycle) alongside β-oxidation, methylcitrate cycle, the carnitine shuttle, the proposed methyl semialdehyde pathway, fatty acid synthesis (FAS), and lipid storage/elongation. Each step is annotated with associated genes, with integrated gene expression change values (log2 fold change–log2FC) visualised as colour-coded boxes indicating direction and magnitude of differential expression. Key compartments include mitochondria (MT), endoplasmic reticulum (ER), lipid droplets (LD), and peroxisomes (PER). *DEG* differentially expressed genes; *LD* lipid droplet; *FFA* free fatty acid; *OCFA* odd-chain fatty acid; *ECFA* even-chain fatty acid; *TAG* triacylglycerol; *SE* sterol esters; *DAG* diacylglycerol; *PA* phosphatidic acid; *LPA* lysophosphatidic acid; *CDP-DAG* cytidine diphosphate-diacylglycerol; *PE* phosphatidylethanolamine; *PC* phosphatidylcholine; *CL*, cardiolipin

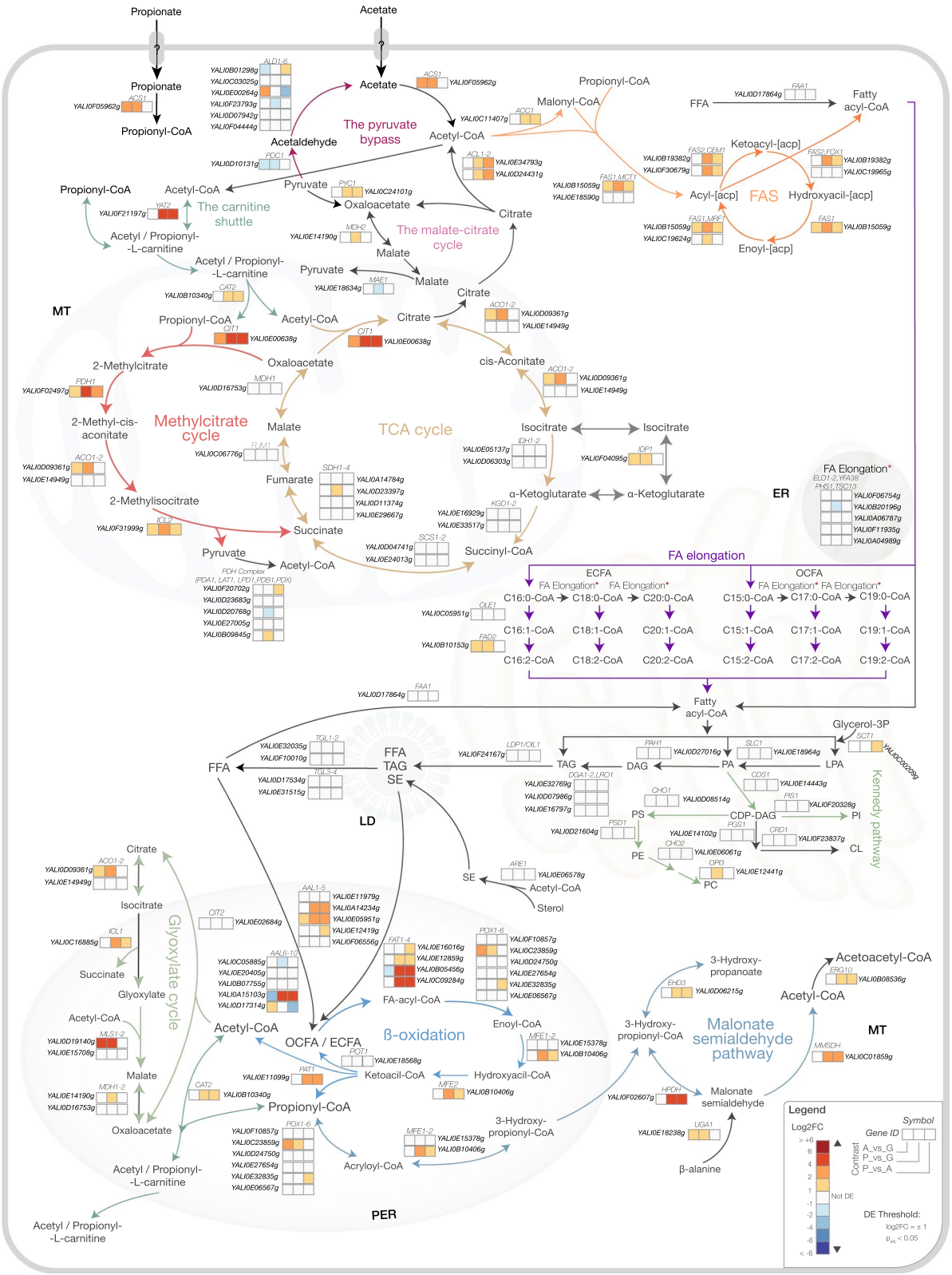

Fig. 5 (See legend on previous page.)

conditions, promoting unsaturated fatty acid synthesis. Increased fatty acid synthesis was also evident by upregulation of the *ACL1* (*YALI0E34793g*) and *ACL2* (*YALI0D24431g*), which provide cytoplasmic acetyl-CoA.

Finally, we observed no transcriptional changes in genes of the pentose phosphate pathway (PPP) enzymes, along with minimal changes in glycolytic/gluconeogenic genes (Additional file 1 Figure S8b). While *PCK1* (*YALI0C16995g*) was upregulated under both acid conditions, *HXK2* (*YALI0E20207g*), *FBP1* (*YALI0A15972g*), *FBA1* (*YALI0E26004g*), *ENO1* (*YALI0F16819g*), and *PYC1* (*YALI0C24101g*) were upregulated only in propionate. As for the glycerol metabolism, distinct expression changes were observed for *S. cerevisiae* orthologs of *ScDAK1* and *ScGCY1* genes (Additional file 1 Figure S8b). Gene *YALI0F01606g*, an ortholog of *ScDAK1*, was upregulated in the propionate and downregulated in the acetate condition, while orthologs of *ScGCY1* were differentially expressed only in the propionate condition, with *YALI0A15906g* and *YALI0D04092g* being upregulated and *YALI0B07117g* downregulated.

As for nitrogen depletion, it has previously been shown that nitrogen limitation activates adenosine monophosphate (AMP) deaminase gene *AMPD* (*YALI0E11495g*), causing a drop in AMP and stopping the TCA cycle by deactivating isocitrate dehydrogenase gene *IDH2* (*YALI0D06303g*), which results in the accumulation of cytosolic citrate. The α-ketoglutarate, on the other hand, then serves as a nitrogen carrier for nitrogen assimilation via glutamate [63, 64]. Our results, however, show no such effect. In the propionate condition, *AMPD* was downregulated, while in acetate, it was not differentially expressed. In contrast, in propionate-grown cells under nitrogen-limited conditions, *GDH1* (*YALI0F17820g*), *GLN1* (*YALI0F00506g*), *GLT1* (*YALI0B19998g*) and *GDH2* (*YALI0E09603g*) showed upregulated expression (Additional file 1 Figure S8c). Interestingly, even though urea was not used as a source of nitrogen, a high induction of *YALI0C15807g*, an ortholog of *S. cerevisiae* urea transporter *ScDUR3*, was observed in both acid conditions, while its paralogs *YALI0E28622g* and *YALI0B04202g* were downregulated. What is more, the orthologs of the *ScDUR12* urea amidolyase had distinct expression patterns, with *YALI0E28622g* being induced in both acid conditions, while *YALI0B14619g* was induced solely in the propionate and repressed in the acetate condition (Additional file 1 Figure S8c). This unexpected induction of urea transport and metabolism genes may reflect a broader stress adaptation mechanisms.

Overall, our data show that propionate assimilation induces a more substantial transcriptional response than acetate, revealing its higher assimilation demands and detoxification strategies under nitrogen limitation.

Discussion

Using transcriptomic analysis, we investigated the adaptive response of *Y. lipolytica* strain EXF-17398 to acetate and propionate as alternative carbon sources under nitrogen-limited conditions. Our findings reveal a substantial transcriptional reprogramming, providing insights into carboxylate uptake, catabolism, and its interplay with lipid synthesis.

Propionic acid triggered a broader transcriptional response in *Y. lipolytica* EXF-17398, with larger DEG sets involving propionic acid contrasts and more DEGs overall, while the transcriptional profile of acetic acid-grown cells was more glucose-like. This transcriptional divergence is also reflected in growth dynamics, as acetic acid is more efficiently consumed, supporting faster growth and a shorter lag phase, as already reported elsewhere [13]. Compared to other carboxylic acids, acetate is preferentially utilised in many yeasts, as it immediately enters central carbon metabolism [2, 12, 13, 63]. On the other hand, lower consumption rates, slower growth, and longer lag phases observed on propionic acid have been attributed to different decarboxylation routes [64, 65], as propionate must first be converted to other intermediates [2, 64]. Interestingly, while cells grown on acetic acid resulted in the fastest growth, final biomass levels across all conditions, including glucose, were relatively similar. This observation suggests that *Y. lipolytica* may compensate for slower growth on propionate through more efficient carbon utilisation or alternative metabolic strategies that ultimately support comparable biomass accumulation. Thus, *Y. lipolytica* strain EXF-17398 efficiently adapted to both acetate- and propionate-based conditions.

The growth of *Y. lipolytica* strain EXF-17398 was strongly pH dependent. During cultivation on carboxylates, pH steadily increased, reaching alkaline conditions at growth completion, as observed in previous studies [66]. Notably, growth on propionic acid accelerated once pH reached 7–8, which agrees with previous findings showing that higher starting pH shortens the lag phase [13, 14, 67]. The observed increase in pH is consistent with known mechanisms of carboxylic acid uptake and intracellular pH regulation in yeasts, where extracellular alkalisation reflects an active acid stress response [68, 69]. At low pH, weak acids diffuse undissociated into cells, but as pH rises, they become deprotonated, reducing passive membrane diffusion [13–15]. Consequently, extracellular alkalisation reflects an active acid stress response, maintaining cytosolic pH homeostasis and facilitating carboxylate utilisation [63].

The carboxylate uptake in yeasts has been primarily attributed to JEN transporters, which facilitate mono- and/or dicarboxylate import through acid/proton-coupled symport mechanisms in many yeasts [16, 50, 51, 53, 54, 66, 70–75]. Consistently, these transporters may contribute to the observed extracellular alkalisation. The *ScJEN1* in *S. cerevisiae* and *CaJEN1* in *C. albicans* were shown to transport propionate [66, 70, 71], with *ScJEN1* also linked to acetate uptake. However, direct evidence for Jen-mediated uptake of these acids in *Y. lipolytica* remains limited, along with their unresolved substrate specificity, as different studies yielded conflicting results. One study proposed that these transporters have broad specificity for both mono- and dicarboxylates, based on heterologous expression of JEN transporters in an *S. cerevisiae jen1Δ ady2Δ* mutant, which restored growth on monocarboxylates (acetate, lactate, pyruvate) and dicarboxylates (malate, α-ketoglutarate, and citrate) [49]. Another study, however, using gene deletion mutants and overexpression profiling in *Y. lipolytica,* has characterised Jen transporters primarily responsible for dicarboxylate utilisation. The sextuple deletion mutant (*jen1-6Δ*) lost the ability to grow on fumarate, malate, and succinate while retaining growth on monocarboxylates acetate, butyrate, pyruvate, and D/L-lactate, as well as dicarboxylates oxaloacetate and citrate. The same study has also suggested that Jen transporter expression in *Y. lipolytica* depends on the available carbon source [41], consistent with our findings. Our data show that all Jen paralogs are expressed on glucose, with *JEN3* and *JEN4* upregulated only in propionate, while *JEN1*, *JEN2*, *JEN5*, and *JEN6* exhibited similar expression patterns in both acid-based conditions. Specifically, *JEN1* and *JEN6* were downregulated, while *JEN2* and *JEN5* were upregulated. Jen transporters thus exhibit pleiotropic phenotypes with overlapping substrate specificities [41, 72, 73], potentially influenced by environmental or regulatory factors beyond substrate availability.

Prior studies have focused primarily on Jen transporters, but our expression data point to the simultaneous involvement of Gpr transporters, homologous to *S. cerevisiae ADY2/ATO1*, *ATO2*, and *ATO3* [46, 76]. *ScJEN1* and *ADY2* have been recognised as primary monocarboxylate transporters in *S. cerevisiae* [73], with *ScJEN1* recognised as a general monocarboxylate/proton symporter, transporting lactate, pyruvate, acetate, and propionate, while *ADY2* is a high-affinity acetate/proton symporter, also transporting propionate and fumarate [66, 70]. Both Sc*JEN1* and *ADY2* transporters have been shown to have a similar expression pattern [54]. This raises the question of whether carboxylate transport in *Y. lipolytica* relies on complementary mechanisms of Jen and Gpr carboxylate transporters rather than being solely managed by the Jen family. Namely, *GPR1* has been shown to restore acetate uptake in a *S. cerevisiae jen1Δ ady2Δ* mutant [76] and has been associated with acetic acid stress adaptation mechanisms [42–46]. We observed that *GPR1* and *GPR6* were upregulated under both acid-based conditions, whereas *GPR2* was downregulated relative to glucose, suggesting divergence in the regulation responses.

Pronounced induction of *JEN5* in propionate and *GPR1* in acetate, with their shared expression patterns along with other paralogs of both gene families and both acid-based conditions, implies *Y. lipolytica* also has two interplayed transport systems of carboxylate uptake. And although previous studies have not directly addressed this, they have, however, shown that the sextuple deletion mutant (*Jen1-6Δ*) retained the ability to grow on monocarboxylates [41], with a limitation that the *Jen1-6Δ* mutant has never been tested on propionate. Thus, our findings highlight their possible complementary roles, with *JEN5* and *GPR1* potentially acting in coordination in response to extracellular pH changes, and being most likely central to propionate and acetate utilisation, respectively, although further integrated studies are needed to define their combined functionality and substrate range.

However, these complementary uptake mechanisms suggest a coordinated metabolic response to carboxylates. Our results highlight that cellular function maintenance is dependent on the efficient coupling of carboxylate uptake with their assimilation through metabolic pathways, including detoxification strategies, energy production, and lipid accumulation. After uptake and activation, acetyl-CoA enters multiple metabolic routes, while propionyl-CoA is a cytotoxic intermediate, possessing significant metabolic burden unless efficiently detoxified [8]. In *Y. lipolytica*, the MCC is the primary detoxification mechanism, converting propionyl-CoA into pyruvate and succinate, intermediates that integrate detoxification with central metabolism [6, 9, 10, 77, 78], also observed in this study. However, under industrial conditions, the MCC may become a metabolic bottleneck due to limited flux capacity or accumulation of toxic intermediates, such as propionyl-CoA, as suggested in recent metabolic engineering studies [78]. The simultaneously upregulated glyoxylate cycle supports carbon conservation and gluconeogenesis by bypassing the CO_2-releasing steps of the TCA cycle (anaplerotic bypass), while continued TCA cycle activity likely sustains energy production and intermediate supply [60]. Propionyl-CoA appears to be transported to mitochondria via the carnitine shuttle. This is supported by a strong upregulation of *CAT2* and *YAT1* genes under the propionate condition and a similar functionality of

propionyl-carnitine transport found in other yeasts, such as *S. cerevisiae* [58, 79], *Candida tropicalis* [11] and *C. albicans* [10]. Previous studies linked *CRC1* to acetyl-carnitine transport but not propionyl-carnitine, while its ortholog *YALI0A20988g* remains untested [59]. In our case, the high upregulation of carnitine acyltransferase genes *CAT2* and *YAT1* did not result in differential expression of its mitochondrial carriers.

An alternative propionyl-CoA detoxification strategy may involve the malonate semialdehyde pathway, previously described in *C. albicans* [10]. In this pathway, propionyl-CoA is converted to 3-hydroxypropionate with enoyl-CoA hydratase/dehydrogenase, followed by a conversion to acetyl-CoA via the activities of 3-hydroxypropionate dehydrogenase encoded by *HPDH* and methylmalonate semialdehyde dehydrogenase encoded by *MMSDH*, orthologs of *C. albicans Hpd1* and *Ald6,* respectively [10]. Under nitrogen depletion, basal β-oxidation of OCFAs contributes to propionyl-CoA formation [9, 80], which may follow one of 3 metabolic routes: (i) entry into the MCC in mitochondria [6, 9, 10, 60, 77], (ii) processing through the malonate semialdehyde pathway [60], or (iii) reincorporation into fatty acid synthesis in the cytosol [9]. The malonate semialdehyde pathway thus likely complements β-oxidation by providing a flexible detoxification route of propionyl-CoA [9].

Under carbon excess and nitrogen depletion, *Y. lipolytica* redirects carbon from biomass formation into lipogenesis [80], by repressing nitrogen-demanding processes and inducing nitrogen-sparing mechanisms [80, 81]. Particularly BCAA catabolism represents an additional supply of propionyl-CoA, acetyl-CoA and nitrogen [11, 60, 61], reinforcing MCC, sustaining the TCA cycle and driving the generation of reducing power (NADPH) for fatty-acid synthesis [9, 10, 80–82]. Thus, accumulation of propionyl-CoA and acetyl-CoA from propionate/acetate metabolism and the BCAA degradation (especially leucine [21, 80, 81]) can lead to carbon overflow ("push" effect), a phenomenon in which excess carbon flux exceeds the biosynthetic capacity of the cell and is redirected toward storage compounds such as lipids. Therefore, driving the carbon flux into the de novo lipogenesis of odd- and even-chain fatty acids [9, 21, 80]. This strategy is analogous to overflow ethanol production in *S. cerevisiae* under nitrogen limitation [80]. Simultaneously, the "pull" is facilitated by the demand for NADPH and redox balance. Growth on acetate drives acetyl-CoA into the TCA/glyoxylate cycle and highlights NADPH generation via oxaloacetate–gluconeogenesis and the oxidative pentose phosphate pathway [19, 83, 84], whereas propionate, assimilated through the MCC, feeds the same pyruvate–oxaloacetate–citrate cycle.

The observed absence of differential expression of core nitrogen regulators (*TOR1/2, SNF1, AMPD, GAT1, GZF3, GLN3, DAL80*) alongside pronounced upregulation of key nitrogen-assimilatory genes (*GDH1/2, GLT1, GLN2*) indicates a nitrogen-regulatory response independent of classical TORC1/NCR-mediated transcriptional control [21, 80]. Instead, under these conditions, *Y. lipolytica* prioritises intracellular nitrogen recycling via the GDH/GLN pathway. The unexpected upregulation of *DUR3* and *DUR12* orthologs without urea or allantoin supplementation further points to a general stress response.

The differences in metabolic pathways between propionate and acetate utilisation highlight the importance of carbon source selection in optimising lipid production in *Y. lipolytica*. While propionate leads to the production of valuable OCFAs, it also poses challenges related to pH stress and carbon flux overflow. In contrast, acetate offers more favourable growth and fewer pH-related issues. Previous studies have shown that co-feeding glucose with carboxylates reduces growth inhibition and supports higher biomass and lipid yields compared to carboxylate-only conditions [4, 85]. In particular, glucose mitigated the inhibitory effects of propionate while it remained a precursor for OCFA synthesis, highlighting co-feeding as a strategy to enhance lipid titres and odd-chain fatty acid production [4]. Beyond acetate, propionate and co-feeding strategies, other carboxylates such as butyrate have also been reported to support lipid accumulation, in some cases exceeding acetate in biomass and lipid yields [85]. Our results indicate that each carboxylate likely triggers a distinct transcriptional response, potentially integrating both de novo and *ex novo* routes of lipid synthesis. Clarifying these metabolic fates will be critical to fully exploit the potential of the carboxylate platform for microbial oil production. Collectively, our findings highlight the critical roles of transport, lipid metabolism, and metabolic reprogramming in enabling *Y. lipolytica* to utilise acetate and propionate for lipid accumulation. Focusing on strain EXF-17398, selected for its superior growth on carboxylates, allowed detailed analysis of transcriptional responses to acetate and propionate, but broader comparative studies will be needed to assess the extent of strain-dependent variability.

Conclusions

This study reveals the transcriptional responses associated with metabolic adaptations of *Yarrowia lipolytica* strain EXF-17398 during growth on acetate and propionate under nitrogen limitation. We highlight the coordinated regulation of the Jen and Gpr

carboxylate transporter families and key detoxification pathways that mitigate propionate toxicity, thereby integrating substrate assimilation with energy metabolism. Our results indicate that de novo lipid synthesis occurs through carbon overflow from acetyl-CoA and propionyl-CoA, complemented by nitrogen recycling and redox balancing, independent of classical nitrogen regulatory mechanisms. These findings provide valuable insights into the metabolic flexibility of *Y. lipolytica* strain EXF-17398, particularly its ability to coordinate carbon and nitrogen metabolism under stress. This knowledge can inform targeted metabolic engineering strategies, such as enhancing MCC flux or optimising transporter expression, to improve lipid production from renewable carboxylate substrates.

Supplementary Information

The online version contains supplementary material available at https://doi.org/10.1186/s13068-025-02713-7.

Additional file 1.

Additional file 2.

Acknowledgements
Not applicable.

Author contributions
E.T.P., M.Ž., D.S.M., C.G. and U.P. conceived the study and designed the experiments. M.Ž., U.H. and D.S.M. performed the experiments and collected the data. M. Ž. performed the RNA-Seq data analysis. C.G. performed the WGS analysis. M.Ž. interpreted the results. M.Ž. drafted the manuscript. E.T.P., C.G., N.Č., C.G.F., D.S.M., and U.P. reviewed and edited the manuscript. U.P. and C.G.F. coordinated the funding acquisition and resource management. All authors have read and agreed to the published version of the manuscript.

Funding
This research was supported by the project OLEOFERM (ERA CoBioTech; PCI2021-121936) financed by MICIU/AEI and NextGenerationEU/PRTR, and by the Slovenian Research and Innovation Agency grants J4-4560, P1-0207 and P1-0198.

Data availability
All reported data are included in the article and its additional information files. The assembled genome and raw expression data have been deposited at GeneBank under the BioProject accession number [PRJNA955139] (https:/www.ncbi.nlm.nih.gov/bioproject/?term=PRJNA955139). Additional supplementary data supporting the findings of this study are available in Additional file 1. Processed results of the differential expression analysis (DEA) are available in Additional file 2.

Declarations

Ethics approval and consent to participate
Not applicable.

Consent for publication
Not applicable.

Competing interests
The authors declare no competing interests.

Author details
[1]Department of Molecular and Biomedical Sciences, Jožef Stefan Institute, Ljubljana, Slovenia. [2]Biotechnical Faculty, Department of Food Science and Technology, University of Ljubljana, Ljubljana, Slovenia. [3]Biotechnological Processes Unit, IMDEA Energy, Madrid, Spain. [4]Biotechnical Faculty, Department of Biology, University of Ljubljana, Ljubljana, Slovenia. [5]Institute of Sustainable Processes, Dr. Mergelina, Valladolid, Spain.

Received: 17 June 2025 Accepted: 19 October 2025
Published online: 10 November 2025

References

1. Zaghen S, Konzock O, Fu J, Kerkhoven EJ. Abolishing storage lipids induces protein misfolding and stress responses in *Yarrowia lipolytica*. J Ind Microbiol Biotechnol. 2023;50:31. https://doi.org/10.1093/JIMB/KUAD031.
2. Žganjar M, Ogrizović M, Matul M, Čadež N, Gunde-Cimerman N, González-Fernández C, et al. High-throughput screening of non-conventional yeasts for conversion of organic waste to microbial oils via carboxylate platform. Sci Rep. 2024;14:1–15. https://doi.org/10.1038/s41598-024-65150-w.
3. Tomás-Pejó E, Morales-Palomo S, González-Fernández C, González-Fernández S. Microbial lipids from organic wastes: Outlook and challenges. Bioresour Technol. 2021;323:124612. https://doi.org/10.1016/j.biortech.2020.124612.
4. Kolouchová I, Schreiberová O, Sigler K, Masák J, Řezanka T. Biotransformation of volatile fatty acids by oleaginous and non-oleaginous yeast species. FEMS Yeast Res. 2015;15:76. https://doi.org/10.1093/FEMSYR/FOV076.
5. Fontanille P, Kumar V, Kumar V, Christophe G, Nouaille R, Larroche C. Bioconversion of volatile fatty acids into lipids by the oleaginous yeast *Yarrowia lipolytica*. Bioresour Technol. 2012;114:443–9. https://doi.org/10.1016/J.BIORTECH.2012.02.091.
6. Park YK, Bordes F, Letisse F, Nicaud JM. Engineering precursor pools for increasing production of odd-chain fatty acids in *Yarrowia lipolytica*. Metab Eng Commun. 2021;12:e00158. https://doi.org/10.1016/J.MEC.2020.E00158.
7. Abreu S, Park YK, Pires de Souza C, Vidal L, Chaminade P, Nicaud JM. Lipid Readjustment in *Yarrowia lipolytica* Odd-Chain Fatty Acids Producing Strains. Biomolecules. 2022;12:1026. https://doi.org/10.3390/BIOM12081026/S1.
8. Bonzanini V, Haddad Momeni M, Olofsson K, Olsson L, Geijer C. Impact of glucose and propionic acid on even and odd chain fatty acid profiles of oleaginous yeasts. BMC Microbiol. 2025;25:1–17. https://doi.org/10.1186/S12866-025-03788-W.
9. Park YK, Dulermo T, Ledesma-Amaro R, Nicaud JM. Optimization of odd chain fatty acid production by *Yarrowia lipolytica*. Biotechnol Biofuels. 2018;11:1–12. https://doi.org/10.1186/S13068-018-1154-4/TABLES/4.
10. Otzen C, Bardl B, Jacobsen ID, Nett M, Brock M. Candida albicans utilizes a modified β-oxidation pathway for the degradation of toxic propionyl-CoA. J Biol Chem. 2014;289:8151–69. https://doi.org/10.1074/JBC.M113.517672/ATTACHMENT/266141E5-1B66-44A7-A1FD-E352E8D522EE/MMC1.XLS.
11. Uchiyama H, Ando M, Toyonaka Y, Tabuchi T. Subcellular localization of the methylcitric-acid-cycle enzymes in propionate metabolism of *Yarrowia zipolytica*. Eur J Biochem. 1982;125:523–7. https://doi.org/10.1111/J.1432-1033.1982.TB06713.X.
12. Morales-Palomo S, González-Fernández C, Tomás-Pejó E. Prevailing acid determines the efficiency of oleaginous fermentation from volatile fatty acids. J Environ Chem Eng. 2022;10:107354. https://doi.org/10.1016/J.JECE.2022.107354.
13. Gao R, Li Z, Zhou X, Cheng S, Zheng L. Oleaginous yeast *Yarrowia lipolytica* culture with synthetic and food waste-derived volatile fatty acids for lipid production. Biotechnol Biofuels. 2017;10:1–15.
14. Gao R, Li Z, Zhou X, Bao W, Cheng S, Zheng L. Enhanced lipid production by *Yarrowia lipolytica* cultured with synthetic and waste-derived high-content volatile fatty acids under alkaline conditions. Biotechnol Biofuels. 2020;13:1–16.

15. Mota MN, Matos M, Bahri N, Sá-Correia I. Shared and more specific genetic determinants and pathways underlying yeast tolerance to acetic, butyric, and octanoic acids. Microb Cell Fact. 2024;23:1–24. https://doi.org/10.1186/S12934-024-02309-0.
16. Lodi T, Diffels J, Goffeau A, Baret PV. Evolution of the carboxylate Jen transporters in fungi. FEMS Yeast Res. 2007;7:646–56. https://doi.org/10.1111/J.1567-1364.2007.00245.X.
17. Wang J, Ledesma-Amaro R, Wei Y, Ji B, Ji XJ. Metabolic engineering for increased lipid accumulation in *Yarrowia lipolytica*—a review. Bioresour Technol. 2020;313:123707. https://doi.org/10.1016/J.BIORTECH.2020.123707.
18. Park YK, Nicaud JM. Metabolic engineering for unusual lipid production in *Yarrowia lipolytica*. Microorganisms. 2020;8:1937. https://doi.org/10.3390/MICROORGANISMS8121937.
19. Liu H, Song Y, Fan X, Wang C, Lu X, Tian Y. *Yarrowia lipolytica* as an oleaginous platform for the production of value-added fatty acid-based bioproducts. Front Microbiol. 2021;11:608662. https://doi.org/10.3389/FMICB.2020.608662.
20. Naveira-Pazos C, Robles-Iglesias R, Fernández-Blanco C, Veiga MC, Kennes C. State-of-the-art in the accumulation of lipids and other bioproducts from sustainable sources by *Yarrowia lipolytica*. Rev Environ Sci Bio/Technol. 2023;22:1131–58. https://doi.org/10.1007/S11157-023-09670-3.
21. Blazeck J, Hill A, Liu L, Knight R, Miller J, Pan A, et al. Harnessing *Yarrowia lipolytica* lipogenesis to create a platform for lipid and biofuel production. Nat Commun. 2014;5:1–10. https://doi.org/10.1038/ncomms4131.
22. Chen S. Ultrafast one-pass FASTQ data preprocessing, quality control, and deduplication using fastp. iMeta. 2023;2(2):e107. https://doi.org/10.1002/IMT2.107.
23. Prjibelski A, Antipov D, Meleshko D, Lapidus A, Korobeynikov A. Using SPAdes de novo assembler. Curr Protoc Bioinform. 2020;70:e102. https://doi.org/10.1002/CPBI.102.
24. Shen W, Sipos B, Zhao L. SeqKit2: a swiss army knife for sequence and alignment processing. iMeta. 2024;3:e191. https://doi.org/10.1002/IMT2.191.
25. Mikheenko A, Prjibelski A, Saveliev V, Antipov D, Gurevich A. Versatile genome assembly evaluation with QUAST-LG. Bioinformatics. 2018;34:i142–50. https://doi.org/10.1093/BIOINFORMATICS/BTY266.
26. Andrews Simon. FastQC A Quality Control tool for High Throughput Sequence Data. 2010. https://www.bioinformatics.babraham.ac.uk/projects/fastqc/. Accessed 20 May 2025.
27. Wingett SW, Andrews S. FastQ screen: a tool for multi-genome mapping and quality control. F1000Res. 2018;7:1338. https://doi.org/10.12688/f1000research.15931.2.
28. Patro R, Duggal G, Love MI, Irizarry RA, Kingsford C. Salmon provides fast and bias-aware quantification of transcript expression. Nat Methods. 2017;14:417–9. https://doi.org/10.1038/nmeth.4197.
29. Danecek P, Bonfield JK, Liddle J, Marshall J, Ohan V, Pollard MO, et al. Twelve years of SAMtools and BCFtools. Gigascience. 2021;10:1–4. https://doi.org/10.1093/GIGASCIENCE/GIAB008.
30. Soneson C, Love MI, Robinson MD. Differential analyses for RNA-seq: transcript-level estimates improve gene-level inferences. F1000Res. 2016;4:1521. https://doi.org/10.12688/f1000research.7563.2.
31. Love MI, Huber W, Anders S. Moderated estimation of fold change and dispersion for RNA-seq data with DESeq2. Genome Biol. 2014;15:1–21. https://doi.org/10.1186/S13059-014-0550-8/FIGURES/9.
32. Liu Y, Li G. Empowering biologists to decode omics data: the Genekitr R package and web server. BMC Bioinform. 2023;24:1–14. https://doi.org/10.1186/S12859-023-05342-9/FIGURES/4.
33. Wu T, Hu E, Xu S, Chen M, Guo P, Dai Z, et al. Clusterprofiler 4.0: a universal enrichment tool for interpreting omics data. Innov (Camb). 2021;2(3):100141. https://doi.org/10.1016/J.XINN.2021.100141.
34. Tamura K, Stecher G, Kumar S. MEGA11: molecular evolutionary genetics analysis version 11. Mol Biol Evol. 2021;38:3022–7. https://doi.org/10.1093/MOLBEV/MSAB120.
35. Xu S, Li L, Luo X, Chen M, Tang W, Zhan L, et al. Ggtree: a serialized data object for visualization of a phylogenetic tree and annotation data. iMeta. 2022;1:e56. https://doi.org/10.1002/IMT2.56.
36. Hallgren J, Tsirigos KD, Damgaard Pedersen M, Juan J, Armenteros A, Marcatili P, et al. DeepTMHMM predicts alpha and beta transmembrane proteins using deep neural networks. bioRxiv. 2022;2022.04.08.487609. https://doi.org/10.1101/2022.04.08.487609.
37. Gutierrez S, Tyczynski WG, Boomsma W, Teufel F, Winther O. MembraneFold: visualising transmembrane protein structure and topology. bioRxiv. 2022;2022.12.06.518085. https://doi.org/10.1101/2022.12.06.518085.
38. Zhou L, Feng T, Xu S, Gao F, Lam TT, Wang Q, et al. ggmsa: a visual exploration tool for multiple sequence alignment and associated data. Brief Bioinform. 2022;23:1–12. https://doi.org/10.1093/BIB/BBAC222.
39. Dragićević MB, Paunović DM, Bogdanović MD, Todorović SI, Simonović AD. ragp: pipeline for mining of plant hydroxyproline-rich glycoproteins with implementation in R. Glycobiology. 2021;30:19–35. https://doi.org/10.1093/GLYCOB/CWZ072.
40. Armenteros JJA, Salvatore M, Emanuelsson O, Winther O, Von Heijne G, Elofsson A, et al. Detecting sequence signals in targeting peptides using deep learning. Life Sci Alliance. 2019. https://doi.org/10.26508/LSA.201900429.
41. Dulermo R, Gamboa-Meléndez H, Michely S, Thevenieau F, Neuvéglise C, Nicaud JM. The evolution of Jen3 proteins and their role in dicarboxylic acid transport in *Yarrowia*. Microbiologyopen. 2015;4:100–20. https://doi.org/10.1002/MBO3.225.
42. Tzschoppe K, Augstein A, Bauer R, Kohlwein SD, Barth G. Trans-dominant mutations in the GPR1 gene cause high sensitivity to acetic acid and ethanol in the yeast *Yarrowia lipolytica*. Yeast. 1999;15:1645–56. https://doi.org/10.1002/(SICI)1097-0061(199911)15:15%3c1645::AID-YEA491%3e3.0.CO;2-G.
43. Augstein A, Barth K, Gentsch M, Kohlwein SD, Barth G. Characterization, localization and functional analysis of Gpr1p, a protein affecting sensitivity to acetic acid in the yeast *Yarrowia lipolytica*. Microbiology (Reading). 2003;149(Pt 3):589–600. https://doi.org/10.1099/MIC.0.25917-0.
44. Matthäus F, Barth G. The Gpr1/Fun34/YaaH Protein Family in the Nonconventional Yeast *Yarrowia lipolytica* and the Conventional Yeast *Saccharomyces cerevisiae*. 2013. https://doi.org/10.1007/978-3-642-38320-5_7.
45. Gentsch M, Barth G. Carbon source dependent phosphorylation of the Gpr1 protein in the yeast *Yarrowia lipolytica*. FEMS Yeast Res. 2005;5:909–17. https://doi.org/10.1016/J.FEMSYR.2005.04.009.
46. Gentsch M, Kuschel M, Schlegel S, Barth G. Mutations at different sites in members of the Gpr1/Fun34/YaaH protein family cause hypersensitivity to acetic acid in *Saccharomyces cerevisiae* as well as in *Yarrowia lipolytica*. FEMS Yeast Res. 2007;7:380–90. https://doi.org/10.1111/J.1567-1364.2006.00191.X.
47. Yan N. Structural biology of the major facilitator superfamily transporters. Annu Rev Biophys. 2015. https://doi.org/10.1146/ANNUREV-BIOPHYS-060414-033901.
48. Quistgaard EM, Löw C, Guettou F, Nordlund P. Understanding transport by the major facilitator superfamily (MFS): structures pave the way. Nat Rev Mol Cell Biol. 2016;17:123–32. https://doi.org/10.1038/nrm.2015.25.
49. Guo H, Liu P, Madzak C, Du G, Zhou J, Chen J. Identification and application of keto acids transporters in *Yarrowia lipolytica*. Sci Rep. 2015;5:1–10. https://doi.org/10.1038/srep08138.
50. Xi Y, Zhan T, Xu H, Chen J, Bi C, Fan F, et al. Characterization of JEN family carboxylate transporters from the acid-tolerant yeast *Pichia kudriavzevii* and their applications in succinic acid production. Microb Biotechnol. 2021;14:1130–47. https://doi.org/10.1111/1751-7915.13781.
51. Casal M, Queirós O, Talaia G, Ribas D, Paiva S. Carboxylic Acids Plasma Membrane Transporters in *Saccharomyces cerevisiae*. Adv Exp Med Biol. 2016;892:229–51. https://doi.org/10.1007/978-3-319-25304-6_9.
52. Soares-Silva I, Ribas D, Sousa-Silva M, Azevedo-Silva J, Rendulić T, Casal M. Membrane transporters in the bioproduction of organic acids: state of the art and future perspectives for industrial applications. FEMS Microbiol Lett. 2020. https://doi.org/10.1093/FEMSLE/FNAA118.
53. Sousa-Silva M, Soares P, Alves J, Vieira D, Casal M, Soares-Silva I. Uncovering Novel Plasma Membrane Carboxylate Transporters in the Yeast *Cyberlindnera jadinii*. J Fungi. 2022;8:51. https://doi.org/10.3390/JOF8010051/S1.
54. Casal M, Paiva S, Queirós O, Soares-Silva I. Transport of carboxylic acids in yeasts. FEMS Microbiol Rev. 2008;32:974–94. https://doi.org/10.1111/J.1574-6976.2008.00128.X.
55. Soares-Silva I, Paiva S, Diallinas G, Casal M. The conserved sequence NXX [S/T]HX [S/T]QDXXXT of the lactate/pyruvate:H+ symporter subfamily defines the function of the substrate translocation pathway. Mol Membr Biol. 2007;24:464–74. https://doi.org/10.1080/09687680701342669.

56. Pronk JT, Van der Linden-Beuman A, Verduyn C, Scheffers WA, Van Dijken JP. Propionate metabolism in *Saccharomyces cerevisiae*: implications for the metabolon hypothesis. Microbiology (N Y). 1994;140:717–22. https://doi.org/10.1099/00221287-140-4-717/CITE/REFWORKS.
57. Luttik MAH, Kötter P, Salomons FA, Van der Klei IJ, Van Dijken JP, Pronk JT. The *Saccharomyces cerevisiae* ICL2 Gene Encodes a Mitochondrial 2-Methylisocitrate Lyase Involved in Propionyl-Coenzyme A Metabolism. J Bacteriol. 2000;182:7007. https://doi.org/10.1128/JB.182.24.7007-7013.2000.
58. Palmieri L, Lasorsa FM, Iacobazzi V, Runswick MJ, Palmieri F, Walker JE. Identification of the mitochondrial carnitine carrier in *Saccharomyces cerevisiae*. FEBS Lett. 1999;462:472–6. https://doi.org/10.1016/S0014-5793(99)01555-0.
59. Messina E, de Souza CP, Cappella C, Barile SN, Scarcia P, Pisano I, et al. Genetic inactivation of the Carnitine/Acetyl-Carnitine mitochondrial carrier of *Yarrowia lipolytica* leads to enhanced odd-chain fatty acid production. Microb Cell Fact. 2023;22:1–16. https://doi.org/10.1186/S12934-023-02137-8/TABLES/2.
60. Huang Z, Wang Q, Khan IA, Li Y, Wang J, Liu X, et al. The methylcitrate cycle and its crosstalk with the glyoxylate cycle and tricarboxylic acid cycle in pathogenic fungi. Molecules. 2023;28:6667. https://doi.org/10.3390/MOLECULES28186667.
61. Rzechonek DA, Szczepańczyk M, Borodina I, Neuvéglise C, Mirończuk AM. Transcriptome analysis reveals multiple targets of erythritol-related transcription factor EUF1 in unconventional yeast *Yarrowia Lipolytica*. Microb Cell Fact. 2024;23:1–17. https://doi.org/10.1186/S12934-024-02354-9/TABLES/1.
62. Dulermo R, Gamboa-Meléndez H, Ledesma-Amaro R, Thevenieau F, Nicaud JM. *Yarrowia lipolytica* AAL genes are involved in peroxisomal fatty acid activation. Biochimica et Biophysica Acta (BBA) - Molecular and Cell Biology of Lipids. 2016;1861:555–65. https://doi.org/10.1016/J.BBALIP.2016.04.002.
63. Robles-Iglesias R, Naveira-Pazos C, Fernández-Blanco C, Veiga MC, Kennes C. Factors affecting the optimisation and scale-up of lipid accumulation in oleaginous yeasts for sustainable biofuels production. Renew Sustain Energy Rev. 2023;171:113043. https://doi.org/10.1016/J.RSER.2022.113043.
64. Vajpeyi S, Chandran K. Microbial conversion of synthetic and food waste-derived volatile fatty acids to lipids. Bioresour Technol. 2015;188:49–55. https://doi.org/10.1016/j.biortech.2015.01.099.
65. Xu Y, Wang X, Li Z, Cheng S, Jiang J. Potential of food waste hydrolysate as an alternative carbon source for microbial oil synthesis. Bioresour Technol. 2022;344:126312. https://doi.org/10.1016/J.BIORTECH.2021.126312.
66. Casal M, Cardoso H, Leão C. Mechanisms regulating the transport of acetic acid in *Saccharomyces cerevisiae*. Microbiology. 1996;142:1385–90. https://doi.org/10.1099/13500872-142-6-1385.
67. Rodrigues G, Pais C. The influence of acetic and other weak carboxylic acids on growth and cellular death of the yeast *Yarrowia lipolytica*. Food Technol Biotechnol. 2000;38:27–32.
68. Sekova VY, Gessler NN, Isakova EP, Antipov AN, Dergacheva DI, Deryabina YI, et al. Redox status of extremophilic yeast *Yarrowia lipolytica* during adaptation to pH-stress. Appl Biochem Microbiol. 2015;51:649–54. https://doi.org/10.1134/S0003683815060137/METRICS.
69. Timoumi A, Cléret M, Bideaux C, Guillouet SE, Allouche Y, Molina-Jouve C, et al. Dynamic behaviour of *Yarrowia lipolytica* in response to pH perturbations: dependence of the stress response on the culture mode. Appl Microbiol Biotechnol. 2017;101:351–66. https://doi.org/10.1007/S00253-016-7856-2.
70. Soares-Silva I, Paiva S, Kötter P, Entian K-D, Casal M, Soares-Silva$ I, et al. The disruption of JEN1 from *Candida albicans* impairs the transport of lactate. Mol Membr Biol. 2004;21:403–11. https://doi.org/10.1080/09687860400011373.
71. Casal M, Paiva S, Andrade RP, Gancedo C, Leão C. The lactate-proton symport of *Saccharomyces cerevisiae* is encoded by JEN1. J Bacteriol. 1999;181:2620–3. https://doi.org/10.1128/JB.181.8.2620-2623.1999.
72. Soares-Silva I, Ribas D, Foskolou IP, Barata B, Bessa D, Paiva S, et al. The *Debaryomyces hansenii* carboxylate transporters Jen1 homologues are functional in *Saccharomyces cerevisiae*. FEMS Yeast Res. 2015;15:94. https://doi.org/10.1093/FEMSYR/FOV094.
73. Alves R, Sousa-Silva M, Vieira D, Soares P, Chebaro Y, Lorenz MC, et al. Carboxylic acid transporters in *Candida* pathogenesis. mBio. 2020. https://doi.org/10.1128/MBIO.00156-20/ASSET/31425CFC-4A71-474F-A04B-C9088256C82E/ASSETS/GRAPHIC/MBIO.00156-20-F0003.JPEG.
74. Queirós O, Pereira L, Paiva S, Moradas-Ferreira P, Casal M. Functional analysis of *Kluyveromyces lactis* carboxylic acids permeases: heterologous expression of *KlJEN1* and *KlJEN2* genes. Curr Genet. 2007;51:161–9. https://doi.org/10.1007/S00294-006-0107-9.
75. Vieira N, Casal M, Johansson B, MacCallum DM, Brown AJP, Paiva S. Functional specialization and differential regulation of short-chain carboxylic acid transporters in the pathogen *Candida albicans*. Mol Microbiol. 2010;75:1337–54. https://doi.org/10.1111/J.1365-2958.2009.07003.X.
76. Ribas D, Soares-Silva I, Vieira D, Sousa-Silva M, Sá-Pessoa J, Azevedo-Silva J, et al. The acetate uptake transporter family motif "NPAPLGL(M/S)" is essential for substrate uptake. Fungal Genet Biol. 2019;122:1–10. https://doi.org/10.1016/J.FGB.2018.10.001.
77. Hapeta P, Rakicka-Pustułka M, Juszczyk P, Robak M, Rymowicz W, Lazar Z. Overexpression of citrate synthase increases isocitric acid biosynthesis in the yeast *Yarrowia lipolytica*. Sustainability. 2020;12:7364. https://doi.org/10.3390/SU12187364.
78. Ma J, Gu Y, Marsafari M, Xu P. Synthetic biology, systems biology, and metabolic engineering of *Yarrowia lipolytica* toward a sustainable biorefinery platform. J Ind Microbiol Biotechnol. 2020;47:845–62. https://doi.org/10.1007/S10295-020-02290-8.
79. Swiegers JH, Dippenaar N, Pretorius IS, Bauer FF. Carnitine-dependent metabolic activities in *Saccharomyces cerevisiae*: three carnitine acetyltransferases are essential in a carnitine-dependent strain. Yeast. 2001;18:585–95. https://doi.org/10.1002/YEA.712.
80. Kerkhoven EJ, Pomraning KR, Baker SE, Nielsen J. Regulation of amino-acid metabolism controls flux to lipid accumulation in *Yarrowia lipolytica*. npj Syst Biol Appl. 2016;2:1–7. https://doi.org/10.1038/npjsba.2016.5.
81. Kerkhoven EJ, Kim YM, Wei S, Nicora CD, Fillmore TL, Purvine SO, et al. Leucine biosynthesis is involved in regulating high lipid accumulation in *Yarrowia lipolytica*. MBio. 2017;8:e00857–17.
82. Zhu Z, Zhang S, Liu H, Shen H, Lin X, Yang F, et al. A multi-omic map of the lipid-producing yeast *Rhodosporidium toruloides*. Nat Commun. 2012;3:1–12. https://doi.org/10.1038/ncomms2112.
83. Spagnuolo M, Hussain MS, Gambill L, Blenner M. Alternative substrate metabolism in *Yarrowia lipolytica*. Front Microbiol. 2018;9:320134. https://doi.org/10.3389/FMICB.2018.01077.
84. Dulermo T, Lazar Z, Dulermo R, Rakicka M, Haddouche R, Nicaud JM. Analysis of ATP-citrate lyase and malic enzyme mutants of *Yarrowia lipolytica* points out the importance of mannitol metabolism in fatty acid synthesis. Biochimica et Biophysica Acta (BBA) - Molecular and Cell Biology of Lipids. 2015;1851:1107–17. https://doi.org/10.1016/J.BBALIP.2015.04.007.
85. Pereira AS, Miranda SM, Lopes M, Belo I. Factors affecting microbial lipids production by *Yarrowia lipolytica* strains from volatile fatty acids: effect of co-substrates, operation mode and oxygen. J Biotechnol. 2021. https://doi.org/10.1016/j.jbiotec.2021.02.014.

Publisher's Note